Localisation of *N*-Acyl Phosphatidylethanolamine Phospholipase D (NAPE-PLD) expression in mouse brain: a new perspective on *N*-acylethanolamines as neural signalling molecules.

MICHAELA EGERTOVÁ[1], GABRIEL M. SIMON[2], BENJAMIN F. CRAVATT[2] AND MAURICE R. ELPHICK[1*]

1. School of Biological and Chemical Sciences, Queen Mary, University of London, Mile End Road, London, E1 4NS, UK.

2. The Skaggs Institute for Chemical Biology and Departments of Cell Biology and Chemistry, The Scripps Research Institute, 10550 North Torrey Pines Road, La Jolla, California 92037, USA.

* Correspondence to:
Prof. M.R. Elphick,
School of Biological & Chemical Sciences,
Queen Mary, University of London,
Mile End Road,
London, E1 4NS, UK.

Tel: 0207 882 5290
Fax: 0208 983 0973
E-mail: M.R.Elphick@qmul.ac.uk

Grant sponsor: Biotechnology and Biological Sciences Research Council, Grant number S19916; Wellcome Trust, Grant number 081428/Z/06/Z.

Abbreviated title: NAPE-PLD expression in mouse brain

Indexing terms: *N*-Acyl Phosphatidylethanolamine Phospholipase D, *N*-acylethanolamines, fatty acid amide hydrolase, anandamide, cannabinoid

ABSTRACT

N-acylethanolamines (NAEs) are membrane-derived lipids that are utilised as signalling molecules in the nervous system (e.g. the endocannabinoid anandamide). A *N*-Acyl Phosphatidylethanolamine Phospholipase D (NAPE-PLD) that catalyses formation of NAEs was recently identified as a member of the zinc metallohydrolase family of enzymes. NAPE-PLD$^{-/-}$ mice have greatly reduced brain levels of long-chain saturated NAEs, but wild-type levels of polyunsaturated NAEs (e.g. anandamide), suggesting an important role for NAPE-PLD in biosynthesis of at least a subset of endogenous NAEs in the mammalian nervous system. To provide a neuroanatomical basis for investigation of NAPE-PLD function, here we have analysed expression of NAPE-PLD in the mouse brain using mRNA *in situ* hybridisation and immunocytochemistry. NAPE-PLD$^{-/-}$ mice were utilised to establish the specificity of probes/antibodies used. The most striking feature of NAPE-PLD expression in the brain was in the dentate gyrus, where a strong mRNA signal was detected in granule cells. Accordingly, immunocytochemical analysis revealed intense NAPE-PLD immunoreactivity in the axons of granule cells (mossy fibres). Intense NAPE-PLD immunoreactivity was also detected in axons of the vomeronasal nerve that project to the accessory olfactory bulb. NAPE-PLD expression was detected in other brain regions (e.g. hippocampus, cortex, thalamus, hypothalamus), but the intensity of immunostaining was weaker than in mossy fibres. Collectively, the data obtained indicate that NAPE-PLD is expressed by specific populations of neurons in the brain and targeted to axonal processes. We suggest that NAEs generated by NAPE-PLD in axons may act as anterograde synaptic signalling

molecules that regulate the activity of post-synaptic neurons.

N-acylethanolamines (NAEs) are a class of lipids that are utilised as signalling molecules in the nervous system and other tissues/organs (Schmid, 2000; Schmid et al., 1990). Probably the most widely known NAE is *N*-arachidonoyl ethanolamine or "anandamide", which is an endogenous ligand for CB_1 cannabinoid receptors in the central nervous system (Devane et al., 1992). Other physiologically active NAEs include the anti-inflammatory lipid *N*-palmitoyl ethanolamine (PEA) and the appetite-suppressing substance *N*-oleoyl ethanolamine (OEA) (Calignano et al., 1998; Jaggar et al., 1998; Lambert et al., 2002; Rodriguez de Fonseca et al., 2001).

The discovery of anandamide as an endocannabinoid has stimulated interest in the mechanisms of biosynthesis of NAEs in mammals. NAE biosynthesis has been proposed to occur via a two-step enzymatic process. First, a Ca^{2+}-activated *N*-acyltransferase transfers the *sn*-1 acyl chain of a phospholipid onto the amine of phosphatidylethanolamine (PE) to generate an *N*-acyl PE (NAPE). Then NAPE is converted by a phospholipase D (PLD) into an NAE and phosphatidic acid (Cadas et al., 1996; Schmid, 2000; Schmid et al., 1990). A Ca^{2+}-independent *N*-acyltransferase that is highly expressed in testis has been discovered recently (Jin et al., 2007) but the molecular identity of a Ca^{2+}-activated *N*-acyltransferase is currently unknown. However, a *N*-Acyl Phosphatidylethanolamine Phospholipase D (NAPE-PLD) that is expressed in the brain has been identified (Okamoto et al., 2004). NAPE-PLD is a 396 amino-acid residue protein in mouse and rat and a member of the zinc metallohydrolase family with a β-lactamase fold. Analysis of the occurrence of NAPE-PLD mRNA/protein in mouse organs/tissues revealed widespread expression but with particularly high levels in

brain and testis, consistent with the distribution of NAPE-PLD enzymatic activity (Okamoto et al., 2004).

Recently, "knockout" mice with the NAPE-PLD gene deleted have been generated to investigate the *in vivo* contribution of NAPE-PLD to NAE biosynthesis (Leung et al., 2006). Consistent with its proposed role in biosynthesis of NAEs, in brain tissue from NAPE-PLD$^{-/-}$ mice there was a five-fold reduction in Ca^{2+}-dependent conversion of NAPEs to NAEs, comprising both saturated and polyunsaturated *N*-acyl chains. However, when the levels of NAEs in NAPE-PLD$^{-/-}$ mice were compared with wild-type littermates, it was found that there was a reduction in NAEs with saturated *N*-acyl chains but no reduction in NAEs with polyunsaturated *N*-acyl chains, including anandamide. Moreover, the most significant reductions were observed for longer NAEs comprising saturated *N*-acyl chains with twenty or more carbon atoms. Collectively, these data indicate that NAPE-PLD is the principal biosynthetic enzyme for long-chain saturated NAEs, but additional enzymatic pathways are likely to contribute to the production of anandamide. Consistent with this premise, a NAPE-PLD-independent pathway for NAE biosynthesis has been postulated wherein de-acylation of the *O*-acyl chains of NAPEs leads to formation of lysoNAPEs and then glycerol-3-phosphate-NAEs (GP-NAEs), which are then converted to NAEs by phosphodiesterase-mediated cleavage of glycerol-3-phosphate (Natarajan et al., 1984). Recently, a (lyso)NAPE lipase that catalyses conversion of NAPEs to GP-NAEs has been purified and identified as α,β-hydrolase-4 (Abhd4) (Simon and Cravatt, 2006).

Another biosynthetic pathway for anandamide has also been characterized in

which phospholipase C catalysed cleavage of NAPE generates phosphoanandamide, which is then dephosphorylated by phosphatases to generate anandamide (Liu et al., 2006). Analysis of enzymes involved in lipopolysaccharide (LPS)-induced anandamide production in macrophages has led to the identification of a phosphatase (PTPN22) as a candidate enzyme in this biosynthetic pathway for anandamide. PTPN22 is also expressed in the brain and in PTPNN22$^{-/-}$ mice enzymatic conversion of phosphoanandamide to anandamide by brain extracts is reduced by comparison with wild-type mice. Therefore, PTPNN22 may contribute to anandamide biosynthesis in the brain and other organs/tissues (Liu et al., 2006).

Our ability to ascribe specific functions to different NAE biosynthetic enzymes is hindered by our limited understanding of their cellular and subcellular distribution in the nervous system and peripheral tissues. A deeper appreciation of the neurophysiological roles of NAPE-PLD would be facilitated by knowledge of its distribution in the brain and in particular which cell types express this enzyme. A preliminary analysis of the regional distribution of NAPE-PLD expression in the rat brain using Western blotting methods and real-time PCR revealed that it is widely distributed but with the highest level of expression in the thalamus (Morishita et al., 2005). However, nothing is known about the identity of cells expressing NAPE-PLD in the brain. Therefore, here we have used mRNA *in situ* hybridisation methods to analyse the distribution of NAPE-PLD mRNA expression in serial sections of the mouse brain, using NAPE-PLD$^{-/-}$ mice to validate the selectivity of the probes used. Furthermore, we have developed novel antibodies to the C-terminal region of mouse NAPE-PLD to

investigate the distribution of the NAPE-PLD protein in the brain and its location in cells expressing the NAPE-PLD gene. NAPE-PLD$^{-/-}$ mice were used to validate the specificity of the immunostaining observed in wild-type mouse brain. The data presented here provide the first detailed analysis of the distribution of NAPE-PLD expression in the brain and a basis for further investigation of the physiological roles of NAPE-PLD in brain function.

MATERIALS AND METHODS

NAPE-PLD mRNA *in situ* hybridisation

Mouse NAPE-PLD cDNA was sub-cloned from a pcDNA3.1(-) vector into pBlueScript SK(+) vector, having established that double-digestion with KpnI and ApaI liberated cDNA inserts. Then digoxygenin (DIG)-labelled antisense and sense RNA probes for NAPE-PLD mRNA were generated using DIG RNA labelling mix (Roche Applied Science, Burgess Hill, UK) and T3 and T7 RNA polymerases (Promega, Southampton, UK; NEB, Hitchin, UK).

Mouse brains dissected from mice perfused with 4% paraformaldehyde (PFA) in phosphate buffered saline (PBS; pH 7.4) were embedded in paraffin wax and serial sections (8 – 10 µm) were cut using a Leica RM 2146 microtome and mounted on Superfrost Plus Micro Slides (VWR, Lutterworth, UK). Following hydration, slides were incubated with proteinase K (20 µg/ml in a buffer comprising 100 mM Tris HCl, pH 7.5; 150 mM NaCl; 0.1% Tween 20) for 20 min at room temperature. Sections were post-fixed with 4% PFA in PBS for 20 min at room temperature and washed in 5 X SSC buffer (20 X SSC = 3 M NaCl, 0.3 M $Na_3C_6H_5O_7$, pH 6.0) followed by 5 X SSC buffer with 0.1% Tween 20 added. Then sections were incubated for 2 h at 60°C with hybridisation buffer (50 % formamide in 5 X SSC, 50 µg/ml yeast RNA, 50 µg/ml heparin, 0.1 % Tween 20; 300 µl per slide). Hybridisation was performed overnight at 60°C in hybridisation buffer containing 800 ng/ml of antisense or sense probes (150 µl per slide covered by a

Parafilm "M" coverslip). Parafilm coverslips were floated off in 5 X SSC buffer and then slides were washed at 60°C in four 30 min steps: 1). 3 parts 50% formamide in 5 X SSC and 1 part 2 X SSC; 2). 1 part 50% formamide in 5 X SSC and 1 part 2 X SSC; 3). 1 part 50% formamide in 5 X SSC and 3 parts 2 X SSC; 4). 2 X SSC. Slides were then washed at room temperature in 0.2 X SSC buffer, followed by two washes in maleic acid buffer (MAB; 0.1 M maleic acid, 0.15 M NaCl, pH 7.5) with 0.1% Tween 20 added. Sections were blocked in 0.5% Blocking Reagent (Roche Applied Science, Burgess Hill, UK) in MAB/0.1%Tween 20 for 1 h at room temperature in a moist chamber. After the blocking solution was drained from slides, 500 µl of anti-DIG alkaline phosphatase-Fab fragments (Roche Applied Science, Burgess Hill, UK) was added, diluted 1:5000 with 0.5% Blocking Reagent in MAB/0.1% Tween 20, and incubated overnight at 4°C in a moist chamber. Slides were washed two times for 10 min in PBS buffer, followed by 10 min in BCL buffer (100 mM Tris, pH 9.5; 100 mM NaCl, 50 mM $MgCl_2$, 0.1 % Tween 20) and then covered with a chromogen mixture consisting of 175 µg/ml 5-bromo-4-chloro-3-indolyl phosphate (VWR, Lutterworth, UK), 337.5 µg/ml nitroblue tetrazolium (VWR, Lutterworth, UK) and lavamisole (Vector Labs. Inc., Burlingame, CA 94010, USA) in BCL buffer. When staining had developed (typically after 6-8 h), slides were washed two times in PBS and then post-fixed with 4% PFA in PBS for 30 min at room temperature. Finally, slides were dehydrated, cleared in xylene and prepared for microscopy by mounting coverslips over VectaMount (Vector Labs. Inc., Burlingame, CA 94010, USA). Sections were viewed under a Leica DMRA2 compound microscope (Leica, Nussloch, Germany) and digital images were captured using a Retiga 1300

monochrome 12 bit camera (QImaging; Burnaby, BC, Canada) and QCapture 1.1.6 software (QImaging) running on a Macintosh G4 computer. Images were then processed to remove dust and assembled into figures using Photoshop 7.0 (Adobe Systems; San Jose, CA, USA) running on a MacBook Pro computer. Images were interpreted and labelled with reference to a mouse brain atlas (Paxinos and Franklin, 2001).

Production and characterisation of antibodies to NAPE-PLD

Antibodies to mouse NAPE-PLD were generated at QMUL using a synthetic peptide antigen (KHGESRYLNTDDRAFEET) comprising the C-terminal region of the protein (Okamoto et al., 2004), which was custom synthesised and purified by the Advanced Biotechnology Centre at Imperial College London. The antigen peptide (NAPE-PLDc) was coupled to thyroglobulin as a carrier protein via the N-terminal lysine residue using glutaraldehyde. Three female New Zealand white rabbits (2282, 2283, 2284) were immunised with NAPE-PLDc-thyroglobulin conjugate (comprising ~100 nmol NAPE-PLDc) emulsified with Freund's complete adjuvant, followed by three monthly booster injections of conjugate (comprising ~ 50 nmol NAPE-PLDc) emulsified with Freund's incomplete adjuvant. Samples of antiserum were collected one week after each booster injection.

Samples of antiserum from each of the bleeds from the three rabbits immunised were tested for the presence of anti-peptide antibodies using dot-blot assays. One µl of a 1 mM solution of the NAPE-PLDc peptide (1 nmol) was pipetted onto a strip of

nitrocellulose membrane alongside negative controls comprising 1 µl of a 1 mM solution of an unrelated peptide (1 nmol) and a 1 µl sample of distilled water. Then after air-drying and washing in PBS (pH 7.4) nitrocellulose membrane strips were blocked in 5% Marvel™ in PBS and incubated individually overnight at 4°C with of each of the antisera diluted 1:250 or 1:500 or 1:1000 in 1% Marvel™/0.05% Tween 20 in PBS (MPBST). After washing in MPBST, strips were incubated for two hours with alkaline phosphatase-labelled goat anti-rabbit immunoglobulins (Vector Labs. Inc., Burlingame, CA 94010, USA) diluted 1:1000 in MPBST and then, after washing with 0.05% Tween 20 in PBS (PBST), bound antibodies were revealed using BCIP/NBT alkaline phosphatase substrate kit IV (Vector Labs. Inc., Burlingame, CA 94010, USA).

Affinity purification of NAPE-PLD antibodies

Dot-blot analysis revealed the presence of anti-peptide antibodies in sera collected after the first, second and third boosts of the NAPE-PLDc-immunised rabbits. Samples of antiserum obtained from rabbits after the third and final boost (2282.3, 2283.3, 2284.3) were subjected to affinity-purification using a column of NAPE-PLDc antigen peptide coupled to AminoLink® Gel (Pierce, Rockford, IL 61105, USA), prepared according to the manufacturer's instructions. Bound antibodies were eluted with 15 ml 100 mM glycine (G; pH 2.5) and then with 15 ml 100 mM triethylamine (T; pH 11.5), which were collected separately into tubes containing 1.5 ml 1M Tris-buffer (pH 8.0).

Western blotting

Brains dissected from both wild-type (NAPE-PLD$^{+/+}$) and knockout (NAPE-PLD$^{-/-}$) mice generated in the Cravatt lab (Leung et al., 2006) were snap frozen on dry-ice and sent to the Elphick lab for Western blot analysis. Following homogenisation on ice in a buffer comprising 2 mM Tris-EDTA, 5 mM $MgCl_2$, 320 mM sucrose and protease inhibitors (Complete Mini; Roche Diagnostics Ltd, Lewes, E. Sussex, UK), particulate material was removed by centrifugation (5500 rpm) for 15 min at 4°C in an Eppendorf 5804R centrifuge. Samples of brain homogenate supernatants (50 or 75 µg protein per lane) were separated by sodium dodecyl sulfate polyacrylamide gel electrophoresis (SDS-PAGE) using a 10% polyacrylamide Tris-glycine gel under reducing conditions, with material from NAPE-PLD$^{+/+}$ and NAPE-PLD$^{-/-}$ mice in alternating lanes. Gels were transblotted to nitrocellulose membrane, which was then cut into strips corresponding to two adjacent lanes. The nitrocellulose membrane strips were incubated with 5% Marvel in PBS for 1 h at room temperature and then incubated individually overnight at 4°C with antisera (1:500) or with one of the six fractions of affinity-purified NAPE-PLD antibody fractions collected (2282.3G, 2282.3T, 2283.3G, 2283.3T, 2284.3G and 2284.3T) diluted 1:5 or 1:10 or 1:15 in MPBST. After washing in MPBST, strips were incubated for two hours with alkaline phosphatase-labelled goat anti-rabbit immunoglobulins (Vector Labs. Inc., Burlingame, CA 94010, USA) diluted 1:1000 in MPBST and then, after washing with 0.05% Tween 20 in PBS (PBST), bound antibodies were revealed using BCIP/NBT alkaline phosphatase substrate kit IV (Vector Labs. Inc., Burlingame, CA 94010, USA).

Immunocytochemistry

Preliminary immunocytochemical analysis of NAPE-PLD expression was performed using brains from mice of the BALB/c strain to establish methodology prior to analysis of brains from male NAPE-PLD-knockout mice (NAPE-PLD$^{-/-}$) and male wild-type littermates (NAPE-PLD$^{+/+}$). Two different methods for preparation of brain sections were tested: 1. Sectioning of paraffin-wax embedded brains fixed with 4% PFA in PBS and post-fixed in Bouin's fixative, as described previously (Egertová et al., 2003) or 2. Sectioning of frozen brains fixed with 4% PFA in PBS. The latter method was found to be preferable for immunocytochemical visualisation of NAPE-PLD expression using the antibodies developed in this study and therefore this method is described in detail below.

Mice were asphyxiated with CO_2 and perfused through the heart with 25 ml of 4% PFA in PBS (pH 7.4) and then brains were removed and transferred to fresh fixative for 1 - 4 days. Then after washing in PBS (2 x 1 hr), brains were cryoprotected overnight with 20% sucrose in PBS. Serial sets of coronal sections (20 µm) of brains were prepared using a Leica freezing microtome (CM3050S) and collected as free-floating sections in PBS containing 0.05% sodium azide. Sections were washed in PBS and incubated with ~3% hydrogen peroxide in PBS for 30 min at room temperature to quench endogenous peroxidase activity. After washing in PBST, sections were blocked with 5% normal goat serum (NGS) in PBS with 0.2% Triton-X100 (PBSTx) for 2 h at room temperature.

Sections were then incubated overnight at 4°C with affinity-purified antibodies to mouse NAPE-PLD (2282.3T) diluted 1:7 - 1:10 in PBSTx with 5% NGS and 0.05% sodium azide added. After washing in PBSTx, slides were incubated for 4 h at room temperature with horseradish-peroxidase conjugated goat anti-rabbit immunoglobulins (Jackson ImmunoResearch). Then after washing in PBS, bound antibodies were revealed using diaminobenzidine (with nickel) as a substrate (Vector Labs. Inc., Burlingame, CA 94010, USA).

Finally, free-floating sections were collected on polysine slides (VWR), dehydrated, cleared in xylene and prepared for microscopy by mounting coverslips over DPX. Images of stained sections were then captured as described above for mRNA *in situ* hybridisation.

RESULTS

Localisation of NAPE-PLD mRNA in mouse brain

The most striking feature of NAPE-PLD expression in mouse brain revealed by mRNA *in situ* hybridisation with DIG-labelled antisense RNA probes was in the hippocampal formation, where intense staining was evident in the granule cell layer of the dentate gyrus (Fig. 1A). No staining was observed in the dentate gyrus in control experiments where a DIG-labelled sense RNA probe was tested on sections of wild-type mouse brains (Fig. 1B) or where the DIG-labelled antisense RNA probe was tested on brains from NAPE-PLD knockout mice (Fig. 1C), demonstrating the specificity of our methods for visualising NAPE-PLD mRNA.

NAPE-PLD expression was also detected in other brain regions, but staining was less intense than in the granule cell layer of the dentate gyrus (Fig. 2A,B). For example, in Fig. 2A compare the staining in the granule cell layer of the dentate gyrus (DG) with staining in the pyramidal cell layer of the hippocampus (Hi) and staining of cells in medial geniculate thalamic nucleus (MG). Expression of NAPE-PLD in other brain regions is described below and illustrated in Fig. 2.

In the hippocampus, staining was present in pyramidal cells throughout all three fields (CA1-CA3), as illustrated in Fig. 2C (CA1; low magnification) and Fig. 2D (CA3; high magnification). In Fig. 2C, note again the higher intensity of staining in the granule cell layer of the dentate gyrus compared to staining in the CA1 pyramidal cell layer.

NAPE-PLD mRNA expression was detected in several regions of the olfactory system. In the olfactory bulb, staining was present in granule cells (Fig. 2E) and periglomerular cells (not shown). In olfactory cortex, staining was present in neuronal cell body layers in the olfactory tubercle (Fig. 2F) and the piriform cortex (Fig. 2G). In the amygdaloid complex, staining was associated with cells in the cortical and medial amygdaloid nuclei (Fig. 2H), whilst the basal (Fig. 2H) and lateral nuclei (not shown) had less staining.

Staining was present in several thalamic nuclei, but at quite low intensity; for examples, see Fig. 1A showing lateral posterior nuclei and Fig. 2A showing the medial geniculate nucleus. In the hypothalamus, staining was evident in cells of the ventromedial nucleus (Fig. 2I). In the neocortex staining was widespread but typically at a low intensity; for example, see Fig. 2J showing an area of visual cortex. In some neocortical areas, however, more intense staining was evident in superficial neuronal cell body layers; for example see Fig. 2K showing retrosplenial cortex. In the cerebellar cortex, staining was present in the granule cell layer and Purkinje cell layer, but not in the molecular layer or white matter (Fig. 2L).

Collectively, the results obtained from mRNA *in situ* hybridisation experiments indicate that NAPE-PLD is expressed by neurons in several brain regions, but with variation between neuronal types in the levels of NAPE-PLD expression. However, for these observations to be interpreted from a functional perspective, immunocytochemical analysis of the distribution of NAPE-PLD protein in brain is necessary.

Western blot analysis of brain homogenates from NAPE-PLD$^{+/+}$ and NAPE-PLD$^{-/-}$ mice with antisera and affinity-purified antibodies to the C-terminal region of mouse NAPE-PLD

Western blot analysis of brain homogenates from NAPE-PLD$^{+/+}$ mice using antisera (2282.3, 2283.3, 2284.3) revealed several immunoreactive bands, ranging in molecular mass from ~25 kDa to ~150 kDa (Fig. 3A,B,C, respectively). The most intensely stained band revealed by the 2282.3 antiserum (Fig. 3A) and the 2284.3 antiserum (Fig. 3C) was located between the 37 kDa and 50 kDa markers, which is consistent with the expected molecular mass for NAPE-PLD (~ 46 kDa). However, this band was also detected in brain homogenates from NAPE-PLD$^{-/-}$ mice, as indeed were other immunoreactive bands in brain homogenates from NAPE-PLD$^{+/+}$ mice (Fig. 3A,C). Thus, the strongly immunoreactive band located between the 37 kDa and 50 kDa markers is not in fact NAPE-PLD but is another protein with a molecular mass very similar to NAPE-PLD that is recognised by antibodies present in the 2282.3 and 2284.3 antisera. Hence, it was necessary to affinity-purify antibodies to the NAPE-PLD C-terminal peptide antigen.

Immunoglobulins eluted with glycine (G) and triethylamine (T) were collected separately and then tested in Western blots of brain homogenates from NAPE-PLD$^{+/+}$ and NAPE-PLD$^{-/-}$ mice (Fig. 3D,E,F). 2282.3(G) labelled a band in NAPE-PLD$^{+/+}$ brain homogenates with a molecular mass of ~46 kDa, which was not detected in NAPE-PLD^{-}

$^{/-}$ brain homogenates (Fig. 3D). However, with 2282.3(G) two strongly immunostained bands located between the 25 kDa and 37 kDa markers were also detected in both NAPE-PLD$^{+/+}$ and NAPE-PLD$^{-/-}$ brain homogenates. 2282.3(T) revealed a single band in NAPE-PLD$^{+/+}$ brain homogenates with the expected molecular mass for NAPE-PLD (~ 46 kDa), which was absent in NAPE-PLD$^{-/-}$ mouse brain homogenates (Fig. 3D). Therefore, the 2282.3(T) fraction appeared to contain antibodies that selectively recognise NAPE-PLD and which we therefore used for immunocytochemical analysis of NAPE-PLD expression in mouse brain (see below). In contrast to 2282.3(T), affinity-purified antibodies derived from the 2283.3 and 2284.3 antisera exhibited cross-reactivity with multiple protein bands that were present in both NAPE-PLD$^{+/+}$ and NAPE-PLD$^{-/-}$ brain homogenates (Fig. 3E,F) and therefore these antibodies were not used for subsequent immunocytochemical studies.

Immunocytochemical localisation of NAPE-PLD in mouse brain

Immunocytochemical analysis of brain sections from NAPE-PLD$^{+/+}$ mice using the 2282.3(T) antibodies revealed a widespread pattern of immunostaining. For example, in Fig. 4A immunoreactivity can be seen in the dentate gyrus (DG), hippocampus (Hi) and the ventral (VTN) and mediodorsal (MD) thalamic nuclei. To assess the specificity of the immunostaining observed in brains from NAPE-PLD$^{+/+}$ mice, the 2282.3(T) antibodies were also tested on sections of brains from NAPE-PLD$^{-/-}$ mice.

The majority of immunostaining observed in brains from NAPE-PLD$^{+/+}$ mice, which is described in more detail below, was not seen in brains from NAPE-PLD$^{-/-}$ mice and therefore can be attributed specifically to expression of NAPE-PLD. For example, Fig. 4B shows a coronal brain section from a NAPE-PLD$^{-/-}$ mouse that is in an intermediate position with respect to the wild-type brain sections shown in Fig. 4A and Fig. 4C; note that the staining of the dentate gyrus, hippocampus and thalamus that can be seen in Fig. 4A is absent in Fig. 4B, demonstrating that this staining can be specifically attributed to NAPE-PLD expression. However, there are structures that are stained in both Fig. 4A and 4B, including the ependyma lining the lateral ventricles (see arrow heads) and the cell bodies and processes of hypothalamic magnocellular neurosecretory cells (see asterisks). This staining is therefore is not attributable to NAPE-PLD expression and must be due to cross-reaction of the NAPE-PLD antibodies with other proteins. Likewise, staining of ventricular ependyma and choroid plexus that can be seen in 4C-F is also not attributable to expression of NAPE-PLD.

The images of NAPE-PLD immunoreactivity (ir) in wild-type mouse brain sections shown in Fig. 4 provide an overview of the most prominent features. In addition to staining associated with the dentate gyrus, hippocampus and thalamus, which was highlighted above, immunoreactivity is also evident in the neocortex, olfactory (piriform) cortex, hypothalamus and amygdaloid complex. More detailed interpretation of the immunostaining, however, requires images of higher magnification than those shown in Fig. 4. Therefore, selected higher magnification images of several regions of the brain are shown in Fig. 5 and described below. In all brain regions where

immunostaining was detected, the staining was not evident in neuronal somata but appeared to be localised in stained fibres surrounding unstained cell bodies and dendrites.

The most striking feature of NAPE-PLD expression in the mouse brain was intense NAPE-PLD-ir present in the polymorphic layer of the dentate gyrus (Fig. 5A), where the pattern of staining was consistent with localisation of NAPE-PLD in mossy fibres, the axons of dentate gyrus granule cells (Longo et al., 2003). Accordingly, analysis of immunostained sections at high magnification revealed that NAPE-PLD-ir was localised in mossy fibre varicosities surrounding unstained cells in the polymorphic layer (Fig. 5B). Immunolabelled mossy fibres were also evident in the stratum lucidum of the CA3 region of the hippocampus (Fig. 5C). Weaker immunostaining was evident in the stratum radiatum and stratum oriens of the hippocampal CA1-CA3 fields (Fig. 5A,D), surrounding unstained somata and dendrites of pyramidal cells (Fig. 5E). In the neocortex, immunostaining was present in superficial layers, but layer VI was only very weakly stained.

In addition to the polymorphic layer of the dentate gyrus, a second region of the brain with very intense immunostaining was the accessory olfactory bulb. Here NAPE-PLD-ir was localised in glomeruli and in axons that project into the accessory olfactory bulb from the vomeronasal nerve (Fig. 5G,H). Immunostaining was also present in the granule cell layer and glomerular layer of the main olfactory bulb, but this staining was less intense than staining in the vomeronasal nerve and the accessory olfactory bulb (Fig. 5H).

Other regions of the forebrain where NAPE-PLD-ir was present included the caudate putamen and the lateral nucleus of the septum (Fig. 5I,J). The majority of thalamic nuclei were immunostained, as can be seen in the low magnification images of Fig. 4. A higher magnification image of immunostaining in the medial and laterial geniculate nuclei is shown in Fig. 5K. Compared to the forebrain, relatively little staining was evident in the midbrain and hindbrain. For example, in the cerebellar cortex very weak immunostaining was present in the molecular layer (Fig. 5L) at an intensity close to the threshold for detection.

DISCUSSION

Here we describe the distribution of NAPE-PLD expression in the mouse brain, utilising mRNA *in situ* hybridisation methods and novel antibodies to a NAPE-PLD C-terminal peptide antigen. Importantly, we have employed use of NAPE-PLD knockout mice (NAPE-PLD$^{-/-}$) for unequivocal evaluation of the specificity of NAPE-PLD antibodies and the immunostaining observed in brains from wild-type mice (NAPE-PLD$^{+/+}$). NAPE-PLD mRNA was detected in the somata of identified neuronal populations in several regions of the brain, including granule cells in the dentate gyrus, olfactory bulb and cerebellar cortex and pyramidal cells in the hippocampus and cortex. NAPE-PLD immunoreactivity was not, however, dectected in the somata of these or any other neuronal populations and the patterns of immunostaining revealed by antibodies to NAPE-PLD indicate that this enzyme is targeted to axons. Although we cannot exclude the possibility that NAPE-PLD is also expressed by glial cells in the brain, the immunostaining obtained provided no evidence of non-neuronal expression.

Importantly, the overall regional distribution of NAPE-PLD mRNA in mouse brain correlated with the distribution of NAPE-PLD protein. For example, both NAPE-PLD mRNA and protein are very abundant in the hippocampal formation but are present at relatively low levels in the cerebellum. Previously, the relative abundance of NAPE-PLD in different regions of the rat brain has been investigated by measurement of NAPE-PLD enzyme activity, Western blotting and real time PCR (Morishita et al., 2005). NAPE-PLD was detected in all rat brain regions analysed but it was most

abundant in the thalamus. Our data also indicate that NAPE-PLD is widely expressed in thalamus, but based on the intensity of immunostaining it appears that in mouse brain NAPE-PLD is more abundant in the hippocampal formation. There may therefore be species differences in the relative abundance of NAPE-PLD in brain regions.

Within regions of the mouse brain mRNA *in situ* hybridisation and immunocytochemistry typically yielded complementary patterns of staining, which can be attributed to the targeting of NAPE-PLD protein to the axons of neuronal somata that express the NAPE-PLD gene. There was also correspondence in the relative intensity of staining revealed by mRNA and protein labelling methods in different neuronal populations. Thus, neurons strongly labelled for NAPE-PLD mRNA had intense NAPE-PLD-ir in their axons (e.g. dentate gyrus granule cells). Conversely, neuronal populations with a weaker mRNA signal (e.g. olfactory bulb granule cells) had correspondingly lower levels of axonal NAPE-PLD-ir.

The brain region with the most striking pattern of NAPE-PLD expression was the dentate gyrus, where a strong NAPE-PLD mRNA signal was detected in granule cells and intense NAPE-PLD immunoreactivity was present in the varicose axons of these cells (mossy fibres). This high level of NAPE-PLD expression in granule cells is of particular interest from a functional perspective because the dentate gyrus is part of the hippocampal formation, which has a fundamental role in some forms of learning and memory as well as having high seizure susceptibility. In hippocampal circuitry, the dendrites of granule cells in the molecular layer of the dentate gyrus receive excitatory input from the entorhinal cortex via the perforant pathway. Then axons of granule cells

(mossy fibres) form *en passant* synapses with neurons such as mossy cells in the polymorphic layer of the dentate gyrus before projecting to the CA3 region of the hippocampus, where they synapse onto the proximal dendrites of pyramidal cells. The presence of intense NAPE-PLD immunoreactivity in the axons of mossy fibres both in the polymorphic layer of the dentate gyrus and in the stratum lucidum of the CA3 field of the hippocampus suggests, therefore, that NAPE-PLD may be involved in regulation of hippocampal synaptic transmission. However, there is at present no direct evidence of such a role and testing this hypothesis may require the development of novel selective inhibitors of NAPE-PLD and/or comparison of hippocampal synaptic transmission in NAPE-PLD$^{+/+}$ and NAPE-PLD$^{-/-}$ mice.

The discovery that NAPE-PLD appears to be principally involved in biosynthesis of saturated, long-chain (e.g. C20:0 and C22:0) NAEs in the brain (Leung et al., 2006) focuses attention on the physiological roles of these lipids in the brain. Based on the observations reported here, it would be of particular interest to analyse the effects of these molecules on synaptic transmission between mossy fibres and mossy cells or CA3 pyramidal cells. We speculate that NAEs generated by NAPE-PLD in the pre-synaptic axon termimals of mossy fibres may function as anterograde synaptic signalling molecules, acting post-synaptically and influencing the activity of mossy cells and CA3 pyramidal cells. Furthermore, although whole-brain levels of anandamide are unaltered in NAPE-PLD$^{-/-}$ mice, it is still possible that NAPE-PLD contributes to anandamide/endocannabinoid signalling, particularly in brain regions where its expression is high (e.g. hippocampal formation).

In animal models of temporal lobe epilepsy sprouting of mossy fibres is observed, with the formation of new synapses between mossy fibre terminals and dendrites of granule cells and inhibitory interneurons occurring in the inner third of the molecular layer of the dentate gyrus (Longo et al., 2003). NAPE-PLD-ir is more intense in the inner third of the molecular layer (IML) than in more superficial layers (Fig. 5D), which may reflect the presence of NAPE-PLD in mossy fibre terminals in the IML. Therefore, an increase in the intensity of NAPE-PLD-ir in the IML may accompany sprouting of mossy fibres in temporal lobe epilepsy. Moreover, the abundance of NAPE-PLD in mossy fibres provides a rationale for investigation of a potential role for NAPE-PLD and the NAEs that it generates in regulation of hippocampal seizure activity.

A second region of the brain with particularly intense NAPE-PLD-ir was the accessory olfactory bulb, where immunostaining was localised in axons projecting from the vomeronasal nerve. These axons originate from the vomeronasal organ, which contains pheromone-sensitive receptor neurons (Brennan, 2001). The presence of NAPE-PLD in vomeronasal axons suggests, therefore, that this enzyme and the NAEs it generates may participate in synaptic mechanisms associated with neural processing of pheromone-stimulated electrical activity in the accessory olfactory bulb. Interestingly, NAPE-PLD-ir is also present in the glomerular layer of the main olfactory bulb and associated with axons derived from olfactory nerve, but this immunostaining is less intense than in the vomeronasal axons associated with the accessory olfactory bulb.

The expression of NAPE-PLD by other neuronal populations in the forebrain is not as striking as in dentate gyrus mossy fibres or vomeronasal axons but nevertheless

important to consider. However, detailed discussion of NAPE-PLD expression in all regions of the brain where it is detected would be excessive and therefore we will focus on a few selected brain regions.

In the hippocampus, NAPE-PLD mRNA is present in pyramidal cells of the CA1-CA3 fields and the pattern of NAPE-PLD immunoreactivity in the hippocampus, with immunostaining surrounding but not localised within pyramidal cell somata or dendrites, is consistent with targeting of the NAPE-PLD protein to the axons of hippocampal pyramidal cells. Thus, NAEs generated by NAPE-PLD may be involved in regulation of excitatory synaptic transmission throughout the hippocampal formation.

In the cortex, NAPE-PLD mRNA expression was clearly evident in pyramidal cells of the olfactory cortex but in the neocortex the intensity of staining for NAPE-PLD mRNA expression was typically rather low. Nevertheless, analysis of NAPE-PLD immunoreactivity in the cortex revealed a pattern of staining consistent with axonal targeting of NAPE-PLD in cortical pyramidal cells. Interestingly, the intensity of NAPE-PLD immunostaining was higher in superficial layers of the neocortex than in layer VI, which may reflect axonal targeting of NAPE-PLD in superficial pyramidal cells that project within the cortex.

In the cerebellar cortex NAPE-PLD mRNA expression was detected in the granule cell layer and weak NAPE-PLD-ir was detected in the molecular layer. These data indicate that the NAPE-PLD gene is expressed by cerebellar granule cells and, consistent with evidence from other brain regions, NAPE-PLD protein is targeted to the axons of these neurons (parallel fibres) in the molecular layer. Furthermore, if NAEs

generated by NAPE-PLD act as anterograde synaptic signalling molecules, as suggested above, then NAEs generated pre-synaptically in parallel fibres may influence the activity of post-synaptic Purkinje cells.

NAEs generated by NAPE-PLD in the brain are potential substrates for the degradative enzyme fatty acid amide hydrolase (FAAH) (Cravatt et al., 2001; Cravatt et al., 1996; Patricelli and Cravatt, 2001). Thus, the physiological half-life of NAEs generated by NAPE-PLD in the brain may be influenced by the proximity and relative abundance of FAAH. It is of interest, therefore, to compare the distribution of NAPE-PLD and FAAH in the mouse brain. The distribution of FAAH expression in the rat and mouse brain has been analysed previously using immunocytochemical techniques (Egertová et al., 2003; Egertová et al., 1998; Egertová et al., 2004; Tsou et al., 1998). Like NAPE-PLD, FAAH is widely expressed but with regional and cellular variation in its relative abundance. FAAH is expressed by many neuronal populations and is also expressed in ventricular ependymal cells and oligodendrocytes. Interestingly, in neurons that express the FAAH gene the FAAH protein is typically targeted to the somatodendritic neuronal compartment (Egertová et al., 2003; Gulyas et al., 2004). Thus, it appears that NAPE-PLD and FAAH are targeted to different sub-cellular compartments in neurons, giving rise to complementary distribution patterns. For example, in the hippocampus FAAH is expressed by pyramidal cells and targeted to their somatodendritic compartment (Egertová et al., 2003; Gulyas et al., 2004), whilst the data presented in this paper indicate that NAPE-PLD is targeted to the axons of pyramidal cells. Likewise, both FAAH and NAPE-PLD are widely expressed in thalamic

nuclei, but FAAH-ir is present in neuronal somata (Egertová et al., 2003) and NAPE-PLD-ir surrounds unstained neuronal somata. This suggests that if NAEs generated by NAPE-PLD in the brain are utilised as anterograde synaptic signalling molecules, then the presence of FAAH in neuronal somata and dendrites may facilitate rapid post-synaptic inactivation of these molecules.

In conclusion, the data presented in this paper provide the first insight into the neuroanatomy of NAPE-PLD expression in the brain and a new perspective on the neural functions of this enzyme and NAEs that it generates. Our finding that NAPE-PLD is targeted to the axons and axon terminals of identified neurons provides a basis for investigation of a potential role for NAEs as mediators of anterograde signalling at synapses.

ACKNOWLEDGEMENTS

We are very grateful to Caroline Brennan and Leonardo Guasti for technical advice on mRNA *in situ* hybridisation methods.

LITERATURE CITED

Brennan PA. 2001. The vomeronasal system. Cell Mol Life Sci 58(4):546-555.

Cadas H, Gaillet S, Beltramo M, Venance L, Piomelli D. 1996. Biosynthesis of an endogenous cannabinoid precursor in neurons and its control by calcium and cAMP. J Neurosci 16(12):3934-3942.

Calignano A, La Rana G, Giuffrida A, Piomelli D. 1998. Control of pain initiation by endogenous cannabinoids. Nature 394(6690):277-281.

Cravatt BF, Demarest K, Patricelli MP, Bracey MH, Giang DK, Martin BR, Lichtman AH. 2001. Supersensitivity to anandamide and enhanced endogenous cannabinoid signaling in mice lacking fatty acid amide hydrolase. Proc Natl Acad Sci U S A 98(16):9371-9376.

Cravatt BF, Giang DK, Mayfield SP, Boger DL, Lerner RA, Gilula NB. 1996. Molecular characterization of an enzyme that degrades neuromodulatory fatty-acid amides. Nature 384(6604):83-87.

Devane WA, Hanus L, Breuer A, Pertwee RG, Stevenson LA, Griffin G, Gibson D, Mandelbaum A, Etinger A, Mechoulam R. 1992. Isolation and structure of a brain constituent that binds to the cannabinoid receptor. Science 258(5090):1946-1949.

Egertová M, Cravatt BF, Elphick MR. 2003. Comparative analysis of fatty acid amide hydrolase and CB1 cannabinoid receptor expression in the mouse brain: evidence of a widespread role for fatty acid amide hydrolase in regulation of endocannabinoid signaling. Neuroscience 119(2):481-496.

Egertová M, Giang DK, Cravatt BF, Elphick MR. 1998. A new perspective on cannabinoid signalling: complementary localization of fatty acid amide hydrolase and the CB1 receptor in rat brain. Proc Biol Sci 265(1410):2081-2085.

Egertová M, Michael GJ, Cravatt BF, Elphick MR. 2004. Fatty acid amide hydrolase in brain ventricular epithelium: mutually exclusive patterns of expression in mouse and rat. J Chem Neuroanat 28(3):171-181.

Gulyas AI, Cravatt BF, Bracey MH, Dinh TP, Piomelli D, Boscia F, Freund TF. 2004. Segregation of two endocannabinoid-hydrolyzing enzymes into pre- and postsynaptic compartments in the rat hippocampus, cerebellum and amygdala. Eur J Neurosci 20(2):441-458.

Jaggar SI, Hasnie FS, Sellaturay S, Rice AS. 1998. The anti-hyperalgesic actions of the cannabinoid anandamide and the putative CB2 receptor agonist palmitoylethanolamide in visceral and somatic inflammatory pain. Pain 76(1-2):189-199.

Jin XH, Okamoto Y, Morishita J, Tsuboi K, Tonai T, Ueda N. 2007. Discovery and characterization of a Ca2+-independent phosphatidylethanolamine N-acyltransferase generating the anandamide precursor and its congeners. J Biol Chem 282(6):3614-3623.

Lambert DM, Vandevoorde S, Jonsson KO, Fowler CJ. 2002. The palmitoylethanolamide family: a new class of anti-inflammatory agents? Curr Med Chem 9(6):663-674.

Leung D, Saghatelian A, Simon GM, Cravatt BF. 2006. Inactivation of N-acyl phosphatidylethanolamine phospholipase D reveals multiple mechanisms for the biosynthesis of endocannabinoids. Biochemistry 45(15):4720-4726.

Liu J, Wang L, Harvey-White J, Osei-Hyiaman D, Razdan R, Gong Q, Chan AC, Zhou Z, Huang BX, Kim HY, Kunos G. 2006. A biosynthetic pathway for anandamide. Proc Natl Acad Sci U S A 103(36):13345-13350.

Longo B, Covolan L, Chadi G, Mello LE. 2003. Sprouting of mossy fibers and the vacating of postsynaptic targets in the inner molecular layer of the dentate gyrus. Exp Neurol 181(1):57-67.

Morishita J, Okamoto Y, Tsuboi K, Ueno M, Sakamoto H, Maekawa N, Ueda N. 2005. Regional distribution and age-dependent expression of N-acylphosphatidylethanolamine-hydrolyzing phospholipase D in rat brain. J Neurochem 94(3):753-762.

Natarajan V, Schmid PC, Reddy PV, Schmid HH. 1984. Catabolism of N-acylethanolamine phospholipids by dog brain preparations. J Neurochem 42(6):1613-1619.

Okamoto Y, Morishita J, Tsuboi K, Tonai T, Ueda N. 2004. Molecular characterization of a phospholipase D generating anandamide and its congeners. J Biol Chem 279(7):5298-5305.

Patricelli MP, Cravatt BF. 2001. Characterization and manipulation of the acyl chain selectivity of fatty acid amide hydrolase. Biochemistry 40(20):6107-6115.

Paxinos G, Franklin KBJ. 2001. The mouse brain in stereotaxic coordinates. London: Academic Press.

Rodriguez de Fonseca F, Navarro M, Gomez R, Escuredo L, Nava F, Fu J, Murillo-Rodriguez E, Giuffrida A, LoVerme J, Gaetani S, Kathuria S, Gall C, Piomelli D. 2001. An anorexic lipid mediator regulated by feeding. Nature 414(6860):209-212.

Schmid HH. 2000. Pathways and mechanisms of N-acylethanolamine biosynthesis: can anandamide be generated selectively? Chem Phys Lipids 108(1-2):71-87.

Schmid HH, Schmid PC, Natarajan V. 1990. N-acylated glycerophospholipids and their derivatives. Prog Lipid Res 29(1):1-43.

Simon GM, Cravatt BF. 2006. Endocannabinoid biosynthesis proceeding through glycerophospho-N-acyl ethanolamine and a role for alpha/beta-hydrolase 4 in this pathway. J Biol Chem 281(36):26465-26472.

Tsou K, Nogueron MI, Muthian S, Sanudo-Pena MC, Hillard CJ, Deutsch DG, Walker JM. 1998. Fatty acid amide hydrolase is located preferentially in large neurons in the rat central nervous system as revealed by immunohistochemistry. Neurosci Lett 254(3):137-140.

FIGURE LEGENDS

Fig. 1. Validation of the specificity of mRNA *in situ* hybridisation methods used to visualise NAPE-PLD expression in mouse brain. **A:** DIG-labelled antisense RNA probes reveal intense staining in the granule cell layer of the dentate gyrus (GrDG) in wild-type mouse brain. Weakly stained cells can also be seen in the lateral posterior thalamic nucleus (LPTN). **B:** No staining is observed when wild-type mouse brain sections are incubated with DIG-labelled sense RNA probes, indicating that the staining observed in A is specific and attributable to NAPE-PLD expression. **C:** No staining is observed when brain sections from NAPE-PLD knockout mice are incubated with DIG-labelled antisense RNA probes, demonstrating that the staining observed in A is specific and attributable to NAPE-PLD expression. *Abbreviations:* GrDG, granule cell layer of dentate gyrus; LPTN, lateral posterior thalamic nucleus; Mol, molecular layer of the dentate gyrus; PoDG, polymorphic layer of the dentate gyrus. Scale bar = 200 µm.

Fig. 2. NAPE-PLD expression in mouse brain as revealed by mRNA *in situ* hybridisation with DIG-labelled antisense RNA probes. **A:** The intense staining of the granule cell layer of the dentate gyrus (DG) can be seen here in contrast to less intense staining in the CA3 pyramidal cell layer of the hippocampus (Hi) and weakly stained cells in the medial geniculate nucleus (MG). **B:** High magnification image of the dentate gyrus showing stained granule cells (GrDG). **C:** The intense staining in the granule cell layer of the dentate gyrus (GrDG) is contrasted here with less intense staining in the CA1

pyramidal cell layer (Py) of the hippocampus. **D:** High magnification image of the CA3 region of the hippocampus showing stained pyramidal cells (Py). **E:** In the olfactory bulb stained granule cells can be seen here in the granule cell layer (GrO) and in the mitral cell layer (Mi). **F:** Stained cells in the olfactory tubercle. **G:** Stained cells in the piriform cortex. **H:** Stained cells in the piriform cortex (Pir) can be seen here in contrast to less intense staining in the cortical (CA) and medial (MA) amygdaloid nuclei and very weak staining in the basomedial amygdaloid nucleus (BMA). **I:** Stained cells in the ventromedial hypothalamic nucleus (VM). **J:** Weakly stained cells in visual neocortex; the asterisk labels layer I of the cortex. **K:** Retrosplenial neocortex, with staining strongest in the superficial cellular layers; the asterisk labels layer I of the cortex. **L:** Cerebellar cortex, with staining evident in both the granule cell layer (GCL) and Purkinje cell layer (PCL) but not in the molecular layer (ML) or white matter (WM). *Abbreviations*: BMA, basomedial amygdaloid nuclei; CA, cortical amygdaloid nuclei; DG, dentate gyrus; EPl, external plexiform layer of the olfactory bulb; GrDG, granule cell layer of the dentate gyrus; GrO, granule cell layer of the olfactory bulb; GCL, granule cell layer of the cerebellar cortex; Hi, hippocampus; LMol, lacunosum moleculare layer; IPl, internal plexiform layer of the olfactory bulb; Mi, mitral cell layer of the olfactory bulb; MA, medial amygdaloid nuclei; MG, medial geniculate thalamic nucleus; ML, molecular layer of the cerebellar cortex; Or, stratum oriens of the hippocampus; Ov, olfactory ventricle; PoDG, polymorphic layer of the dentate gyrus; Pir, piriform cortex; PCL, Purkinje cell layer; Py, pyramidal cell layer of the hippocampus; Rad, stratum

radiatum of the hippocampus; Tu, olfactory tubercle; VP, ventral pallidum; WM, white matter. Scale bar = 50 µm in B, D, L; 100 µm in C, E, F, G, I, J, K; 200 µm in A, H.

Fig. 3. Characterisation of antisera (A, B, C) and affinity-purified antibodies (D, E, F) to mouse NAPE-PLD by Western blot analysis of brain homogenates from NAPE-PLD$^{+/+}$ and NAPE-PLD$^{-/-}$ mice. NAPE-PLD antisera [**A**: 2282.3(AS), **B**: 2283.3(AS), **C**: 2284.3(AS)] label bands in wild-type (+/+) brains with a wide range of molecular masses, including an intensely stained band between 37 kDa and 50 kDa markers with a molecular mass similar to that expected for mouse NAPE-PLD (~46 kDa). However, all the stained bands evident in wild-type brains, including the intensely stained band between 37 kDa and 50 kDa markers, are also detected in brains from knockout animals (-/-) and therefore are not NAPE-PLD, demonstrating the necessity for affinity-purification of antibodies to the NAPE-PLD C-terminal peptide antigen. **D:** Affinity-purifed antibodies derived from the 2282.3 antiserum and eluted with glycine (G) or triethylamine (T) label a ~ 46 kDa band in wild-type (+/+) brain homogenates that it is not present in knockout (-/-) brain homogenates and which therefore must be NAPE-PLD (see arrow). The 2282.3(G) antibodies also label two bands between the 25 kDa and 37 kDa markers that are present in both wild-type and knockout brain homogenates. However, 2282.3(T) antibodies only stain the ~ 46 kDa band corresponding to NAPE-PLD and therefore these antibodies were selected for immunocytochemical analysis of NAPE-PLD expression in mouse brain. **E, F:** Affinity-purifed antibodies derived from the 2283.3 and 2284.3 antisera also label a ~46 kDa band corresponding to NAPE-PLD

(see arrows). However, these antibodies also cross-react with other proteins and therefore were not used for immunocytochemical analysis of NAPE-PLD expression in mouse brain.

Fig. 4. Immunoreactivity in coronal sections of mouse forebrain (A,C,D,E,F) attributable to NAPE-PLD expression by comparative immunocytochemical analysis NAPE-PLD$^{-/-}$ mice (B). **A:** Immunostaining in anterior regions of the dentate gyrus (DG), hippocampus (Hi) and thalamus (MD, VTN). **B**: Immunostaining is almost completely absent in this coronal section of NAPE-PLD knockout mouse brain positioned intermediate with respect to the sections of wild-type brain shown in A and C. The only staining present is in ventricular ependyma (arrow head) and in hypothalamic magnocellular neurons (*) and, with the exception of these features, all of the staining in wild-type brain (A, C, D, E, F) is specifically attributable to NAPE-PLD expression. **C, D, E, F:** Here, in addition to immunostaining in the hippocampal formation (DG, Hi) and thalamus (Gus, LG, MD, MG, Po, VP), NAPE-PLD immunoreactivity is also present in the neocortex (NC), piriform cortex (Pir), amygdaloid complex (AmC) and hypothalamus (Hy). *Abbreviations*: AmC, amygdaloid complex; CPu, caudate putamen; DG, dentate gyrus; Gus, gustatory thalamic nucleus; Hi, hippocampus; ic, internal capsule; LG, lateral geniculate thalamic nucleus; MD, mediodorsal thalamic nucleus; MG, medial geniculate thalamic nucleus; NC, neocortex; Pir, piriform cortex; Po, posterior thalamic nucleus; VP, ventroposterior thalamic nucleus; VTN, ventral thalamic nuclei. Scale bar = 500 µm.

Fig. 5. Localisation of NAPE-PLD immunoreactivity in mouse brain regions. **A:** In the hippocampal formation intense immunostaining is present in the polymorphic layer of the dentate gyrus (PoDG). Strong staining is also present in the stratum lucidum (see white asterisk) in the CA3 field of the hippocampus. Weaker staining is evident in the molecular layer of the dentate gyrus (Mol), the stratum oriens (Or) and the stratum radiatum (Rad) in the CA1 - CA3 fields of the hippocampus and the laterodorsal thalamic nucleus (LDTN). **B:** High magnification image showing immunostained mossy fibre axons with varicosities surrounding unstained cells (see asterisks) in the polymorphic layer of the dentate gyrus. **C:** Intensely immunostained mossy fibre axons can be seen here in the stratum lucidum (SLu) in the CA3 field of the hippocampus. Less intense staining can be seen in the stratum radiatum (Rad) and stratum oriens (Or). Note the absence of immunostaining in cell bodies of the pyramidal cell layer (Py). **D:** Here the intensity of immunostaining in hippocampal and neocortical (NC) layers can be compared; the external capsule (ec) marks the boundary between the neocortex and hippocampus. Note that in the molecular layer of the dentate gyrus (Mol) the intensity of staining in the inner zone (arrow head) is slightly stronger than in the outer zone of this layer. **E:** Immunostaining in the CA1 field of the hippocampus; note that in the stratum radiatum (Rad) immunostaining surrounds the unstained primary dendrites of pyramidal cells. **F:** Immunstaining in neocortex (auditory); note that staining is more intense in superficial layers (Sup) of the cortex than in layer VI. **G:** Intense immunostaining is present in the vomeronasal nerve (VN) and its axonal projections

into the glomerular layer of the accessory olfactory bulb (AOB); staining in lateral orbital cortex can also be seen in this image. **H:** Immunostaining is present in the olfactory nerve (ON) and the glomerular layer (Gl) of the main olfactory bulb but is less intense than in the vomeronasal nerve (VN); weak staining is also evident here in the granule cell layer of the olfactory bulb. **I:** Low magnification view of anterior forebrain showing immunostaining in cingulate (Cg) and motor (M1, M2) cortex, septum (S) and caudate putamen (CPu). **J:** In the septum immunostaining is present in the lateral septal nuclei (LS) but not in the medial septal nucleus (MS). **K:** Immunostaining in posterior thalamic nuclei (LG, MG, LP); note the difference in the intensity of thalamic staining and immunostaining in the adjacent dentate gyrus (DG). **L:** In the cerebellar cortex, very weak immunostaining is evident in the molecular layer (ML). *Abbreviations*: AOB, accessory olfactory bulb; cc, corpus callosum; cg, cingulated cortex; CPu, caudate putamen; DG, dentate gyrus; ec, external capsule; EPl, external plexiform layer of the olfactory bulb; GCL, granule cell layer of the cerebellar cortex; GrDG, granule cell layer of the dentate gyrus; Gl, glomerular layer of the olfactory bulb; GrO, granule cell layer of the olfactory bulb; IPl, internal plexiform layer of the olfactory bulb; LDTN, laterodorsal thalamic nucleus; LG, lateral geniculate thalamic nucleus; LMol, lacunosum moleculare layer; LO, lateral orbital cortex; LP, lateroposterior thalamic nucleus; LS, lateral septal nucleus; M1, primary motor cortex; M2, secondary motor cortex; Mi, mitral cell layer of the olfactory bulb; MA, medial amygdaloid nuclei; MG, medial geniculate thalamic nucleus; ML, molecular layer of the cerebellar cortex; MOB, main olfactory bulb; Mol, molecular layer of the dentate gyrus; MS, medial septal nucleus; ON,

olfactory nerve; Or, stratum oriens of the hippocampus; NC, neocortex; PoDG, polymorphic layer of the dentate gyrus; Pir, piriform cortex; PCL, Purkinje cell layer; Py, pyramidal cell layer of the hippocampus; Rad, stratum radiatum of the hippocampus; S, septum; SLu, stratum lucidum of the hippocampus;. Scale bars = 15 μm in B; 50 μm in C, E, F; 100 μm in G, H; 200 μm in A, D, J, K, L; 500 μm in I.

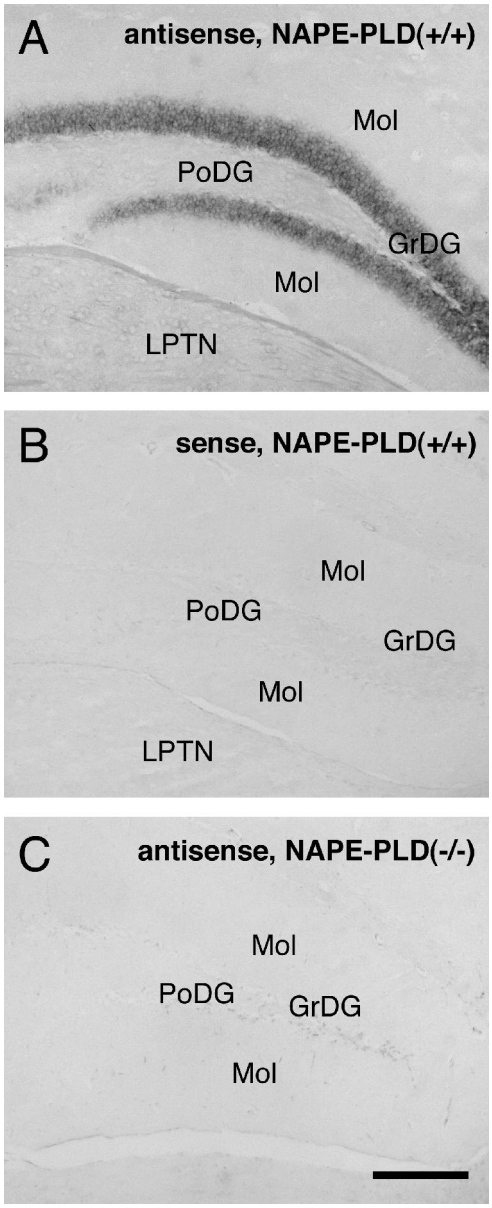

Fig. 1. Validation of the specificity of mRNA in situ hybridisation methods used to visualise NAPE-PLD expression in mouse brain. A: DIG-labelled antisense RNA probes reveal intense staining in the granule cell layer of the dentate gyrus (GrDG) in wild-type mouse brain. Weakly stained cells can also be seen in the lateral posterior thalamic nucleus (LPTN). B: No staining is observed when wild-type mouse brain sections are incubated with DIG-labelled sense RNA probes, indicating that the staining observed in A is specific and attributable to NAPE-PLD expression. C: No staining is observed when brain sections from NAPE-PLD knockout mice are incubated with DIG-labelled antisense RNA probes, demonstrating that the staining observed in A is specific and attributable to NAPE-PLD expression. Abbreviations: GrDG, granule cell layer of dentate gyrus; LPTN, lateral posterior thalamic nucleus; Mol, molecular layer of the dentate gyrus; PoDG, polymorphic layer of the dentate gyrus. Scale bar = 200 µm.
108x268mm (300 x 300 DPI)

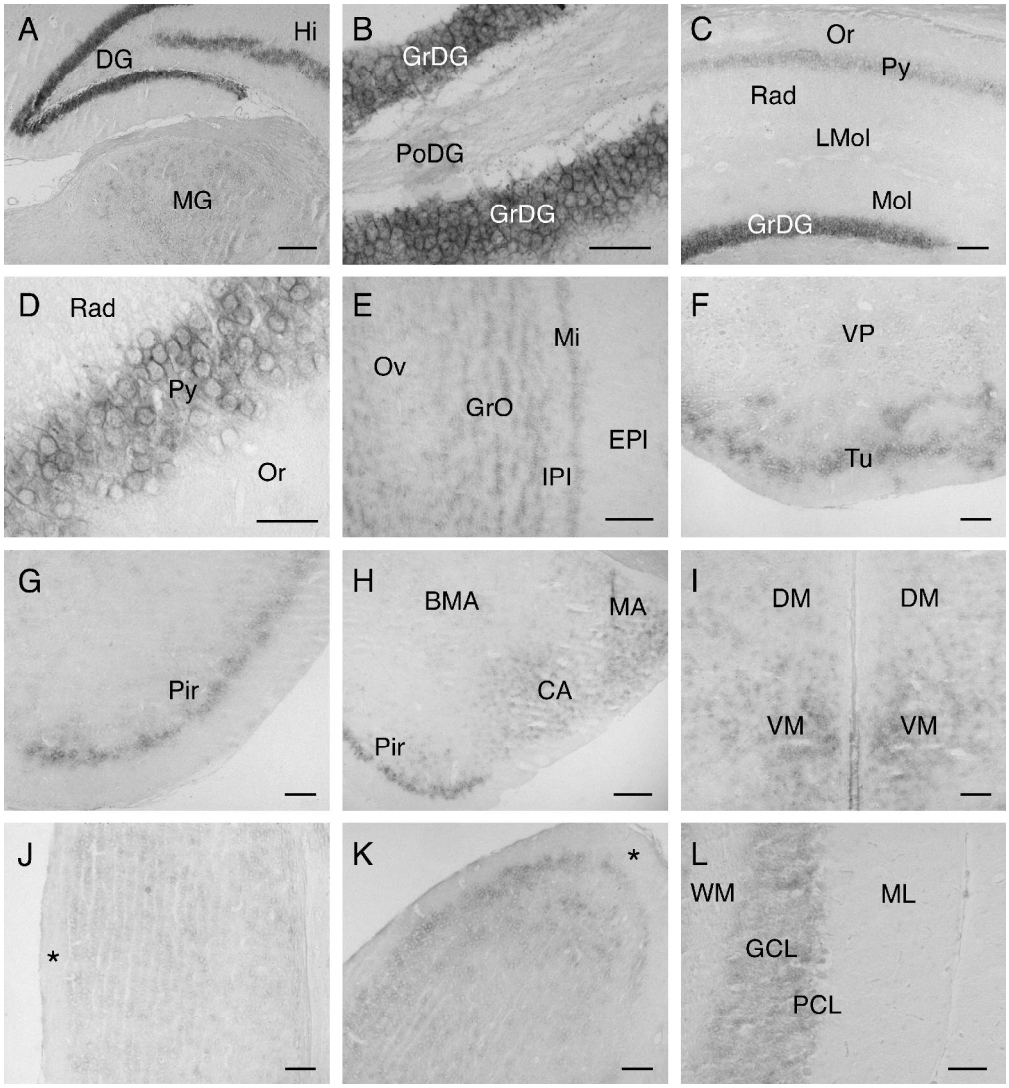

Fig. 2. NAPE-PLD expression in mouse brain as revealed by mRNA in situ hybridisation with DIG-labelled antisense RNA probes. A: The intense staining of the granule cell layer of the dentate gyrus (DG) can be seen here in contrast to less intense staining in the CA3 pyramidal cell layer of the hippocampus (Hi) and weakly stained cells in the medial geniculate nucleus (MG). B: High magnification image of the dentate gyrus showing stained granule cells (GrDG). C: The intense staining in the granule cell layer of the dentate gyrus (GrDG) is contrasted here with less intense staining in the CA1 pyramidal cell layer (Py) of the hippocampus. D: High magnification image of the CA3 region of the hippocampus showing stained pyramidal cells (Py). E: In the olfactory bulb stained granule cells can be seen here in the granule cell layer (GrO) and in the mitral cell layer (Mi). F: Stained cells in olfactory tubercle. G: Stained cells in the piriform cortex. H: Stained cells in the piriform cortex (Pir) can be seen here in contrast to less intense staining in the cortical (CA) and medial (MA) amygdaloid nuclei and very weak staining in the basomedial amygdaloid nucleus (BMA). I: Stained cells in the ventromedial hypothalamic nucleus (VM). J: Weakly stained cells in visual neocortex; the asterisk labels layer I of the cortex. K: Retrosplenial neocortex, with staining strongest in the

superficial cellular layers; the asterisk labels layer I of the cortex. L: Cerebellar cortex, with staining evident in both the granule cell layer (GCL) and Purkinje cell layer (PCL) but not in the molecular layer (ML) or white matter (WM). Abbreviations: BMA, basomedial amygdaloid nuclei; CA, cortical amygdaloid nuclei; DG, dentate gyrus; EPl, external plexiform layer of the olfactory bulb; GrDG, granule cell layer of the dentate gyrus; GrO, granule cell layer of the olfactory bulb; GCL, granule cell layer of the cerebellar cortex; Hi, hippocampus; LMol, lacunosum moleculare layer; IPl, internal plexiform layer of the olfactory bulb; Mi, mitral cell layer of the olfactory bulb; MA, medial amygdaloid nuclei; MG, medial geniculate thalamic nucleus; ML, molecular layer of the cerebellar cortex; Or, stratum oriens of the hippocampus; Ov, olfactory ventricle; PoDG, polymorphic layer of the dentate gyrus; Pir, piriform cortex; PCL, Purkinje cell layer; Py, pyramidal cell layer of the hippocampus; Rad, stratum radiatum of the hippocampus; Tu, olfactory tubercle; VP, ventral pallidum; WM, white matter. Scale bar = 50 µm in B, D, L; 100 µm in C, E, F, G, I, J, K; 200 µm in A, H.

333x359mm (300 x 300 DPI)

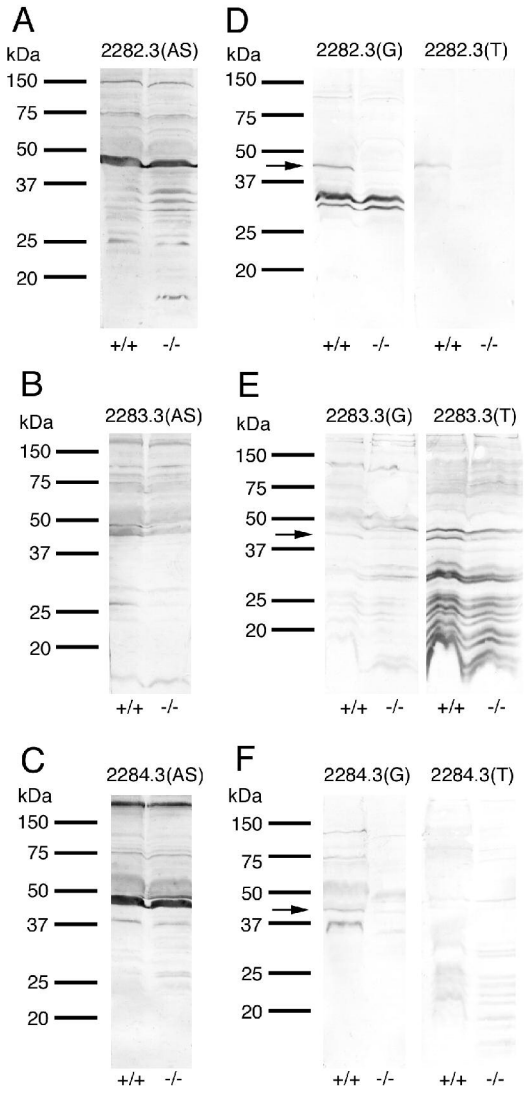

Fig. 3. Characterisation of antisera (A, B, C) and affinity-purified antibodies (D, E, F) to mouse NAPE-PLD by Western blot analysis of brain homogenates from NAPE-PLD+/+ and NAPE-PLD-/- mice. NAPE-PLD antisera [A: 2282.3(AS), B: 2283.3(AS), C: 2284.3(AS)] label bands in wild-type (+/+) brains with a wide range of molecular masses, including an intensely stained band between 37 kDa and 50 kDa markers with a molecular mass similar to that expected for mouse NAPE-PLD (~46 kDa). However, all the stained bands evident in wild-type brains, including the intensely stained band between 37 kDa and 50 kDa markers, are also detected in brains from knockout animals (-/-) and therefore are not NAPE-PLD, demonstrating the necessity for affinity-purification of antibodies to the NAPE-PLD C-terminal peptide antigen. D: Affinity-purifed antibodies derived from the 2282.3 antiserum and eluted with glycine (G) or triethylamine (T) label a ~ 46 kDa band in wild-type (+/+) brain homogenates that it is not present in knockout (-/-) brain

homogenates and which therefore must be NAPE-PLD (see arrow). The 2282.3(G) antibodies also label two bands between the 25 kDa and 37 kDa markers that are present in both wild-type and knockout brain homogenates. However, 2282.3(T) antibodies only stain the ~ 46 kDa band corresponding to NAPE-PLD and therefore these antibodies were selected for immunocytochemical analysis of NAPE-PLD expression in mouse brain. E, F: Affinity-purifed antibodies derived from the 2283.3 and 2284.3 antisera also label a ~46 kDa band corresponding to NAPE-PLD (see arrows). However, these antibodies also cross-react with other proteins and therefore were not used for immunocytochemical analysis of NAPE-PLD expression in mouse brain.
118x219mm (300 x 300 DPI)

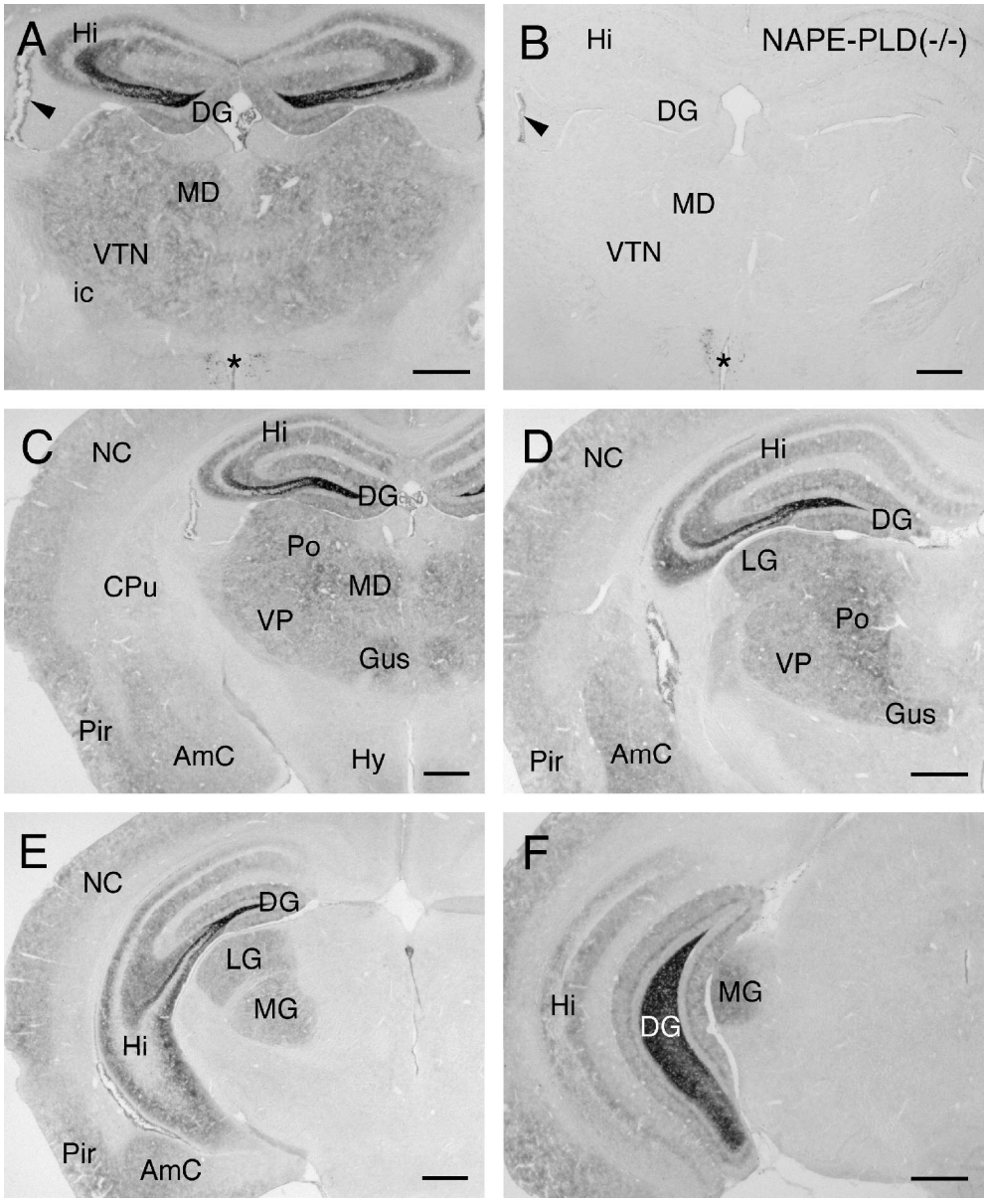

Fig. 4. Immunoreactivity in coronal sections of mouse forebrain (A,C,D,E,F) attributable to NAPE-PLD expression by comparative immunocytochemical analysis NAPE-PLD-/- mice (B). A: Immunostaining in anterior regions of the dentate gyrus (DG), hippocampus (Hi) and thalamus (MD, VTN). B: Immunostaining is almost completely absent in this coronal section of NAPE-PLD knockout mouse brain positioned intermediate with respect to the sections of wild-type brain shown in A and C. The only staining present is in ventricular ependyma (arrow head) and in hypothalamic magnocellular neurons (*) and, with the exception of these features, all of the staining in wild-type brain (A, C, D, E, F) is specifically attributable to NAPE-PLD expression. C, D, E, F: Here, in addition to immunostaining in the hippocampal formation (DG, Hi) and thalamus (Gus, LG, MD, MG, Po, VP), NAPE-PLD immunoreactivity is also present in the neocortex (NC), piriform cortex (Pir), amygdaloid complex (AmC) and hypothalamus (Hy). Abbreviations: AmC,

amygdaloid complex; CPu, caudate putamen; DG, dentate gyrus; Gus, gustatory thalamic nucleus; Hi, hippocampus; ic, internal capsule; LG, lateral geniculate thalamic nucleus; MD, mediodorsal thalamic nucleus; MG, medial geniculate thalamic nucleus; NC, neocortex; Pir, piriform cortex; Po, posterior thalamic nucleus; VP, ventroposterior thalamic nucleus; VTN, ventral thalamic nuclei. Scale bar = 500 µm.
220x268mm (300 x 300 DPI)

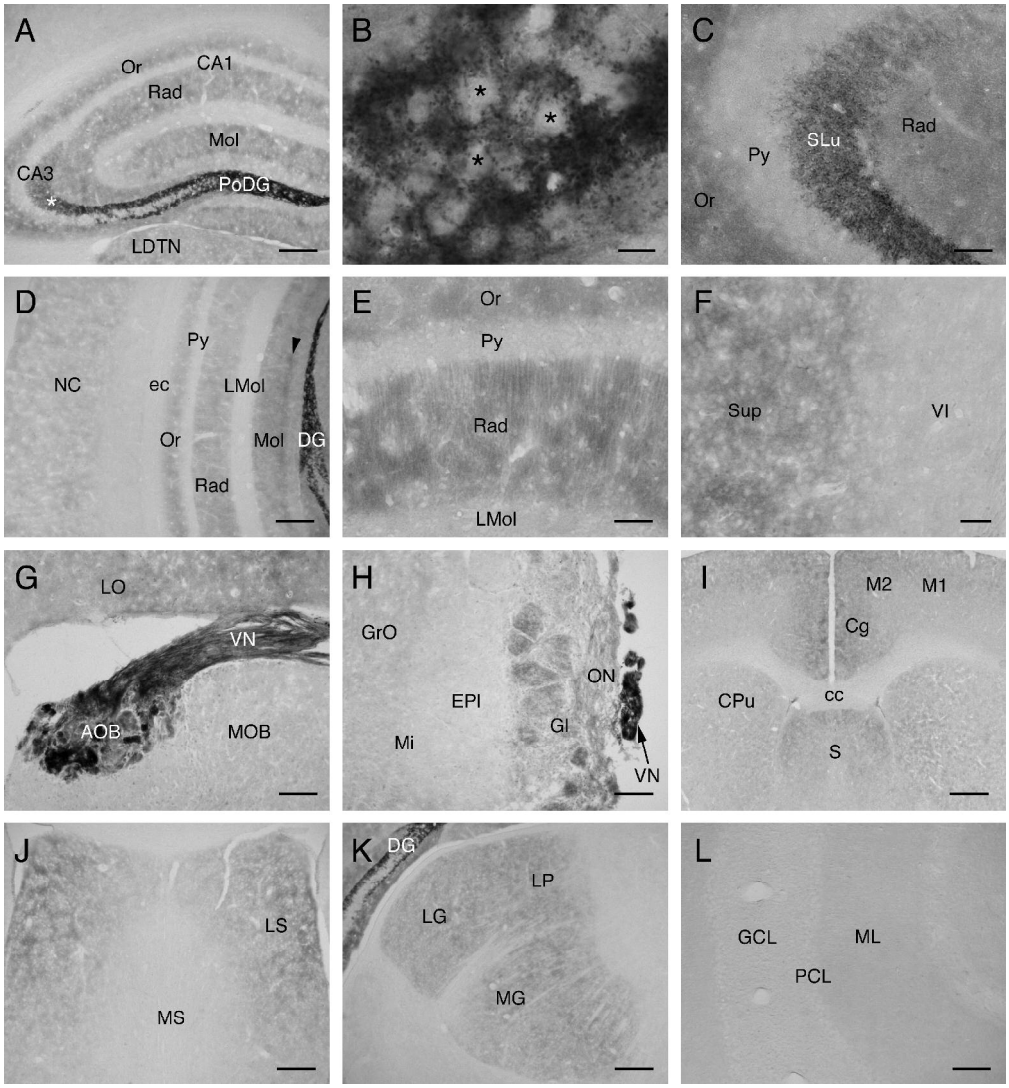

Fig. 5. Localisation of NAPE-PLD immunoreactivity in mouse brain regions. A: In the hippocampal formation intense immunostaining is present in the polymorphic layer of the dentate gyrus (PoDG). Strong staining is also present in the stratum lucidum (see white asterisk) in the CA3 field of the hippocampus. Weaker staining is evident in the molecular layer of the dentate gyrus (Mol), the stratum oriens (Or) and the stratum radiatum (Rad) in the CA1 - CA3 fields of the hippocampus and the laterodorsal thalamic nucleus (LDTN). B: High magnification image showing immunostained mossy fibre axons with varicosities surrounding unstained cells (see asterisks) in the polymorphic layer of the dentate gyrus. C: Intensely immunostained mossy fibre axons can be seen here in the stratum lucidum (SLu) in the CA3 field of the hippocampus. Less intense staining can be seen in the stratum radiatum (Rad) and stratum oriens (Or). Note the absence of immunostaining in cell bodies of the pyramidal cell layer (Py). D: Here the intensity of immunostaining in hippocampal and neocortical (NC) layers can be compared; the external capsule (ec) marks the boundary between the neocortex and hippocampus. Note that in the molecular layer of the dentate gyrus (Mol) the intensity of staining in the inner zone (arrow head) is slightly stronger than in the outer zone of this layer. E: Immunostaining in the CA1 field

of the hippocampus; note that in the stratum radiatum (Rad) immunostaining surrounds the unstained primary dendrites of pyramidal cells. F: Immunstaining in neocortex (auditory); note that staining is more intense in superficial layers (Sup) of the cortex than in layer VI. G: Intense immunostaining is present in the vomeronasal nerve (VN) and its axonal projections into the glomerular layer of the accessory olfactory bulb (AOB); staining in lateral orbital cortex can also be seen in this image. H: Immunostaining is present in the olfactory nerve (ON) and the glomerular layer (Gl) of the main olfactory bulb but is less intense than in the vomeronasal nerve (VN); weak staining is also evident here in the granule cell layer of the olfactory bulb. I: Low magnification view of anterior forebrain showing immunostaining in cingulate (Cg) and motor (M1, M2) cortex, septum (S) and caudate putamen (CPu). J: In the septum immunostaining is present in the lateral septal nuclei (LS) but not in the medial septal nucleus (MS). K: Immunostaining in posterior thalamic nuclei (LG, MG, LP); note the difference in the intensity of thalamic staining and immunostaining in the adjacent dentate gyrus (DG). L: In the cerebellar cortex, very weak immunostaining is evident in the molecular layer (ML).
333x359mm (300 x 300 DPI)